Long-wavelength 256x256 QWIP Hand-held Camera

S. 1). Gunapala, J. K. Liu, M. Sundaram, S. V. Bandara, C. A. Shott*, T. Hoelter*, P. D. Maker, and R. E. Muller

Center for Space Microelectronics Technology, Jet Propulsion Laboratory, California Institute of Technology, Pasadena, CA 91109.

* Amber, A Raytheon Company, Goleta, CA 93117.

ABSTRACT

in this paper, we discuss the development of very sensitive long wavelength infrared (I .WIR) GaAs/AlxGa1 -xAs quantum well infrared photodetectors (QWI f's), fabrication of random reflectors for efficient light coupling, and the demonstration of first hand-held kmg-wavelength 256 x 2.56 QWIP focal plane array camera. Excellent imagery, with a noise. equivalent differential temperature (NEAT) of 25 mK has been achieved.

KEYWORDS

multi-quantum- well, intersubband, infrared detectors, king- wavelength, GaAs, focal plane array, infrared camera

INTRODUCTION

There are several applications that require long wavelength, large, uniform, reproducible, low cost, low]/f noise, low power dissipation, and radiation hard infrared (IR) focal plane arrays (FPAs). For example, the absorption lines of many gas molecules, such as ozone, water, carbon monoxide, carbon dioxide, and nitrous oxide occur in the wavelength region from 3 to 18 pm. Thus, IR imaging systems that operate in the long wavelength IR (1 .WIR) region (6 - J 8 pm) arc required in many space applications such as monitoring global atmospheric temperature profiles, relative humidity profiles,

cloud characteristics, and the distribution of minor constituents in the atmosphere which are being planned for NASA's Earth Observing System [1]. In addition, 8 - 15 μm FPAs would be very useful in detecting cold objects such as ballistic missiles in midcourse (when a hot rocket engine is not burning most of the emission peaks are in the 8-15 μm IR region) [2]. The GaAs based Quantum Well Infrared Photodetector (QWIP) [3,4,5] is a potential candidate for such spaceborne and ground based applications and it can meet all of the requirements mentioned above. for this spectral region.

Fig. 1 shows the schematic conduction band diagram of a typical *bound-to-con tinuum* QWIP [6] which utilizes bound-to-continuum intersubband absorption. By carefully designing the quantum well structure, as well as the light coupling to the detector, it is possible to optimize the material to have an optical response in the desired spectral range and determine the spectral response shape [7]. in QWIPs, the dark current originates from three different mechanisms [8]. As shown in Fig. 1, the dark current arising from the first process is due to quantum mechanical tunneling from well to well through the $Al_xGa_{1-x}As$ barriers (sequential tunneling). This process is independent of temperature. Sequential tunneling dominates the dark current at very low temperatures (<30 K). The second mechanism is thermally assisted tunneling which involves a thermal excitation and tunneling through the tip of the barrier into the continuum energy levels. This process governs the dark current at medium temperatures. The third mechanism is classical thermionic emission and it dominates the dark current at higher temperatures (>55 K for 9 μm cutoff QWIPs). Consequently, for Q WIPs operating at higher temperatures the last mechanism is the major source of dark current [8]. Therefore, the LWIR FPA we have discussed here in detail consisted of *bound-to-quasibound* QWIPs [9]. The advantage of the bound-to-quasibound QWIP over the bound-to-continuum QWIP [9] is that in the case of a bound-to-quasibound QWIP the energy barrier for thermionic emission is the same as it is for photoionization as shown in Fig. **2.** In the case of the bound-to-cont inuum QWIP shown in Fig. 2 the energy barrier for the thermionic emission is about 6 meV less than the photoionization energy. Thus, the dark current of bound-to-quasibound QWIPs is reduced by a factor of 3 (i.e., $I_d \propto e^{-\frac{\Delta E}{kT}} \approx e^{-1}$ for T = 70 K) compared with bound-to-continuum QWIPs operating at the same peak wavelength.

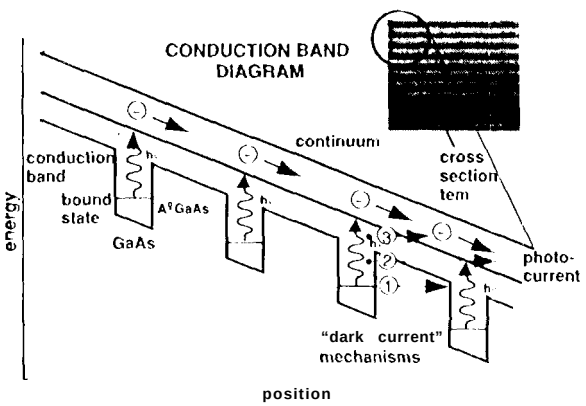

Fig. 1 Schematic diagram of the conduction band in a bound-to- continuum QWIP in an externally applied electric field. Absorption of IR photons can photoexcite electrons from the ground state of the quantum well into the continuum, causing a photocurrent. Three dark current mechanisms are also shown: ground state tunneling (1); thermally assisted tunneling (2); and thermionic emission (3).

TEST STRUCTURE RESULTS

The device structure consists of 50 periods, each period containing a 45 Å wc]] of GaAs (doped n = 4x1017 cm^{-3}) and a 500 Å barrier of $Al_{0.3}Ga_{0.7}As$, sandwiched between 0.5 μm GaAs top and bottom contact layers doped $n = 5x\ 10^{17}\ cm^{-3}$, grown on a semi-insulating GaAs substrate by molecular beam epitaxy (MBE). Then a ().7 " μm thick GaAs cap layer on top of a 300 Å $Al_{0.3}Ga_{0.7}As$ stop-etch layer was grown *in situ* on top of the device structure to fabricate the light coupling optical cavity. The MBE grown QWIP structure was processed into 200 *pm* diameter mesa test structures (area= 3.14 x 10-4 cm^2) using wet chemical etching, and Au/Ge ohmic contacts were evaporated onto the top and bottom contact layers. The dark current-voltage curves of the QWIP were measured as a function of temperature from T = 30-90 K and the T = 70 K curve is shown in Fig. 2 with the dark current-vol[agc curve of a 8.5 μm peak bound-to-continuum QWIP. The virtual excited level of this bound-to-conti nuum QWIP is 6 meV above the $Al_xGa_{1-x}As$ barrier. Theoretically this should give a factor of 3 higher dark current and it closely agrees with the experimental value of a factor of 4 higher dark current at bias V_B = -2V.

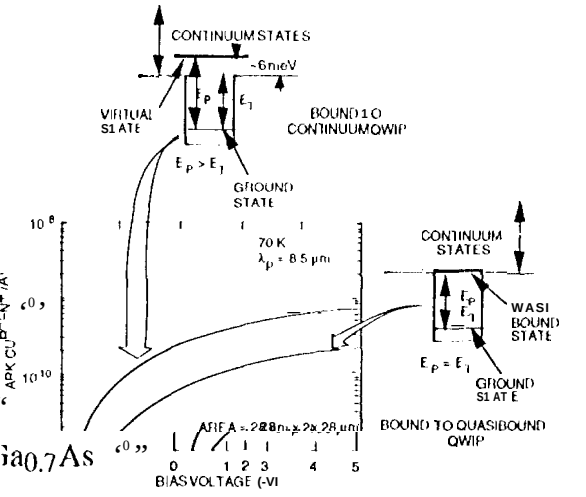

Fig. 2 Comparison of dark currents of bound-to-continuum and bound- to-quasibound LWIR QWIPs as a function of **bitts** *voltage at temperature T = 70 K. Data were taken with a 200 μm diam test structure and normalized to 28x28 μm2* **pixel.**

The responsivit y spectra of these detectors were measured using a 1000 K blackbody source and a grating monochromator. The absolute peak responsivities (R_p) of the detectors were measured using a calibrated blackbody source. The detectors were back illuminated through a 45° polished facet [7]. Figure 3 shows typical photoresponse curves of long wavelength bound-to-conti nuum, and bound-to-quasibound test QWIPs at temperature T = 77 K. The absor pti on and photoresponse curves Of the bound-to-conti nuum QWI 1's arc much broader than those of the bound-to-qu asibound QWIPs. This is because the first excited state, being in the continuum, is broader in the former than in the latter. The responsivity of the detector peaks at 8.5 μm and the peak responsivity (R_p) of the detector is 300 mA/W at bias V_B = -3 V. The spectral width and the cutoff wavelength arc $\Delta\lambda / \lambda$ = 10% and λ_c = 8.9 pm respectivel y. The measured absolute peak responsivit y of the detector is small up to about V_B = -0,5 V. Beyond that it increases nearly linearly with bias reaching R_P = 380 mA/W at V_B = -5 V. This type of behavior of responsivity versus bias is typical for a bound-to-quasibound QWIP. The peak quantum

efficiency was 6.9% at bias V_B = -1 V (lower quantum efficiency is due to the lower well doping density) for a **45°** double pass.

The current noise i_n was measured using a spectrum analyzer and the photoconductive gain g was experimentally determined using [10] $g = i_n^2 / 4eI_DB + 1/2N$, where B is the measurement bandwidth and N is the number of quantum wells. The photoconductive gain of the detector reached **0.98** at V_B =-5 V. Since the gain of QWIP is inversely proportional to the number of quantum wells N, the better comparison would be the well capture probability p_c, which is directly related to the gain [1 1] by $g = 1/Np_c$. The calculated wc]] capture probabilities arc 25% at low bias (i.e., V_B = -1 V) and 2% at high bias (i.e., V_B = -5 V) which together indicate the excellent hot-electron transport in this device structure. The peak detectivity is defined as $D_p^* = R_p \sqrt{AB} / i_n$, where R_P is the peak responsivity, A is the area of the detector and A = 3.14×10^{-4} cm^2. The measured peak detectivity at bias V_B = -3.2 V and temperature T = 70 K is 2.3x 10^{11} cm√Hz/W. The bias dependent detectivit y of the detector is shown in Fig. **4. These** detectors show background limited performance (BLIP) at bias V_B = -2 V and temperature '1' = **72** K for 300 K background with f/2 optics.

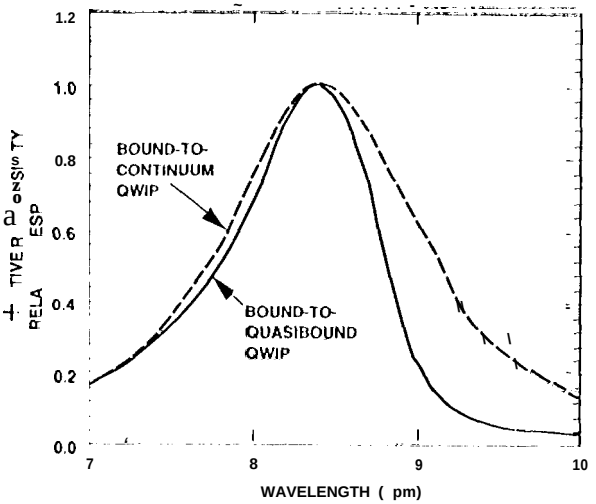

Fig. 3 Typical photoresponse curves of bound-to-continuum and bound-to-quasibound QWIPs at temperature T = 77 K.

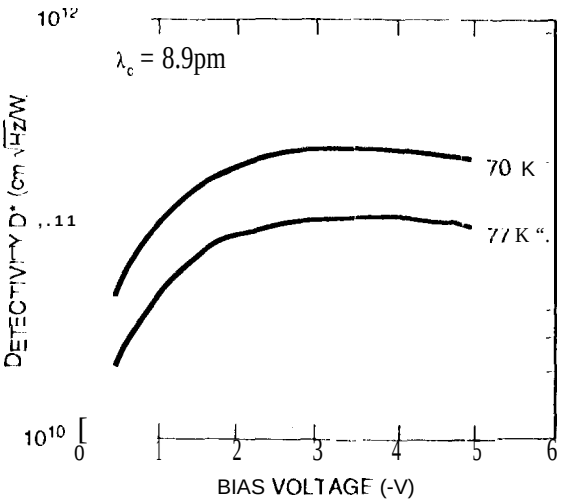

Fig. 4 Detectivity as a function of bias voltage at temperatures T = 70 and 77 K.

LIGHT COUPLING

in order to be absorbed by the electrons in the quantum wells, the incoming light should have an electric field component in the quantum well direction, i .e., in the growth direction, normal to the layers. Only in this situation is the electric field of the light coupled to the quantized electron momentum, enabling a photon to excite an electron and get absorbed in the process. Light being a transverse wave (whose electric field is perpendicular to the direction of travel), this selection rule means that light

striking the layers normally (the most direct way to illuminate an imaging array of detectors) is not absorbed. If the light is sent through the thin (~ 500 μm) edge of the detector it can be absorbed since it now has a component of its electric field in the correct direction. The edge is sometimes given a 45° wedge and the incident light focused normally on the polished edge. facet [7]. Both schemes result in incident light being piped late.rally through the detector. This clearly limits the configuration of detectors to linear arrays and single elements. For imaging, it is necessary to be able (o couple light uniformly to two-dimensional arrays of detectors. An elegant way to couple normally incident light to an imaging array of QWIPs is to usc a grating to bend some of the light inside the detectors.

This is accomplished by putting a special reflector on the detector top and illuminating the detector from the back. If the reflector is a smooth mirror, it is useless: the normally incident light passes through the detector, strikes the mirror, and is reflected straight back out of the back side with none of the light being absorbed by the confined electrons. To be useful, the mirror has to be rough (cm the scale of the wavelength of the light in the detector's GaAs material). This roughness may be either periodic or random (Fig. 5). A rough mirror scatters or sprays the incident light back in a cone (i.e., the roughness ensures that the angle of reflection no longer equals the angle of incidence). The details of the cone depend on the details of the roughness. This cone now strikes the bottom side. '1'hose rays that arc within a critical angle of the normal (17° for the GaAs-air interface) refract or escape back into the air. The rest suffer total internal reflection with tbc back surface acting as a smooth mirror. The internall y reflected rays arc once again reflected off the top rough mirror. What happens next depends on whether the roughness of the top mirror is periodic or random. If it is periodic, the top mirror will scatter or bend these rays so that they arc all normal to the quantum wc]] layers again. These rays pass through the detector and out of the back side. A *randomly* roughened mirror, on the other hand, will randomly reflect or scatter a]] the rays internally reflected cm to it from the bottom side. each time, thereby allowing the incident Ii ght to bounce back and forth bet wccn the. detector top and back surfaces several times. Only light within a 17° (from normal) cone. escapes out of the back side. Clever design can reduce the amount of light in the escape cone but cannot eliminate it altogether. For instance, if the random reflector is designed with Iwo levels of rough surfaces having the same areas but locate.d a quarter wavelength ($\lambda_{GaAs}/4$) apart, the *normally* reflected light intensities from the top and bottom surfaces of the reflector arc equal and 180° out of phase. This maximizes the destructive interference at normal reflection and lowers light leakage through the escape cone.

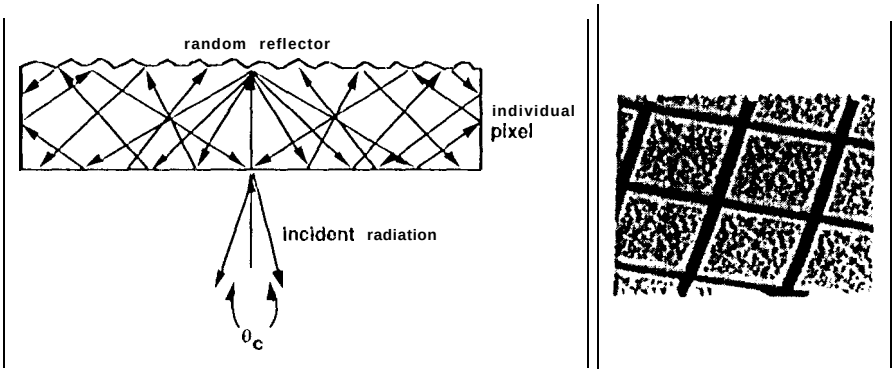

Fig. 5 (a) Schematic side view of a thin QWIP pixel with a random reflector. Ideally all the radiation is trapped except for a small fraction which escape through the escape cone (defined by critical angle Qc), (b) Random reflectors on pixels in a focal plane army.

On each pass through the detector following the first reflection off the top rough mirror, some of the light is absorbed by the confined electrons since most of the light rays now have an electric field Component in the correct direction (normal to the quantum well layers). A periodically roughened mirror thus yields two useful passes; a randomly roughened mirror offers several. One measure of the resulting efficiency of the detector in absorbing photons is its responsivity (the photocurrent for a given incident photon flux). Under identical conditions, a top reflector with one-dimensional periodic roughness will give a QWIP about the same responsivity that it would have if illuminated through a 45° edge facet; both the reflector with two-dimensional periodic roughness as WC]] as the random reflector will approximately double. this responsivity. Squeezing the maximum light trapping ability from the reflector requires increasing the detector aspect ratio, i.e., the. ratio of detector diameter to height, a design feature accomplished by thinning the ~ 500 μm thick GaAs substrate on top of which the detector material is grown, to about zero. The resulting optical cavity is calculated and measured to improve the responsivity of a QWIP with a random reflector significantly over the 45" case [1 1]. '1'binning enhances the responsivities of the QWIPs with 1 D and 2D periodically rough reflectors to be respectively about 2 and 4 limes better than the 45° case. The random reflector is fabricated on the QWIPs using standard photolithography and CCl_2F_2 selective dry etching. The advantage of the photolithographic process over a completely random process is the ability to accurately control feature size and preserve the pi xel-to-pixel uniformit y necessary for very sensitive imaging focal plane arrays.

IMAGING ARRAYS

The imaging arrays were fabricated as follows. After the random reflector array was defined by lithography and dry etching, the photoconductive QWIPs of the 256x256 pixel FPAs were. fabricate.d by wet chemical etching of trenches (to isolate each QWIP pixel from its neighbors) through the photosensitive $GaAs/Al_xGa_{1-x}As$ multi-quantum well layers into the 0.5 μm thick doped GaAs bottom contact layer. The pitch of the FPA is 38 μm; the actual pixel size is 28 μm x 28 pm. The random

reflectors on the tops of the detectors were then covered with Au/Ge and Au for Ohmic contact and reflection. Figure 6 shows a picture of twenty-five 256x256 pixel QWIP FPAs on a ~-inch GaAs wafer, produced by the Jet Propulsion laboratory. Indium bumps were then evaporated on the tops of the detectors for Si readout circuit (ROC) hybridization. A single QWIP FPA was chosen and hybridized or mated (via an indium bump-bonding process as shown in Fig. 7) to a matching, 256x256 pixel CMOS multiplexer (Amber AE- 166), and biased at V_B = -1 V.

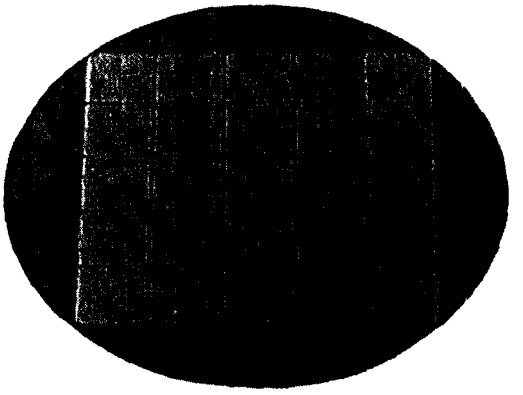

Fig. 6 Twenty five 256.x256 QWIP focal plane arrays on a 3 in. GaAs wafer.

At temperatures below 72 K, the signal-to-mist ratio of the system is limited by array non-uniformity, multiplexer readout noise, and photo current (photon flux) misc. At temperatures above 72 K, temporal noise duc to the QWIP's higher dark current becomes the limitation. The FPA was back-illuminated through the flat thinned substrate membrane (thickness ≈ 1300 Å). The measured mean NEAT of the FPA with no lens was 26 mK at an operating temperature of '1' = 70 K and bias V_B = -1 V, for a 300 K background. This initial array gave excellent images with 99.98% of tbc pixels working (number of dead pixels ≈ 10), demonstrating the high yield of GaAs technology.

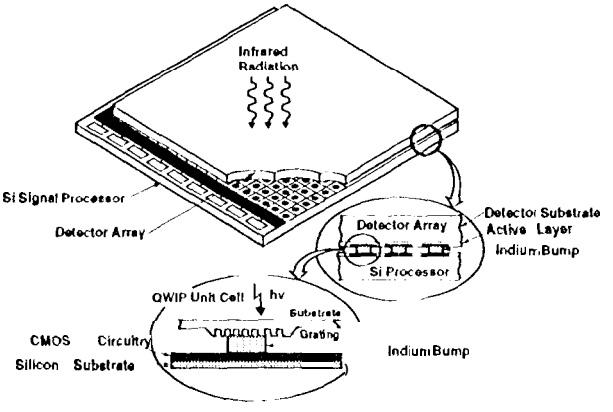

Fig. 7 Cross section Of 256x256 QWIP FPA and silicon CMOS multiplexer hybrid.

HAND-HELD CAMERA

A **256x256** QWIP FPA hybrid was mounted on to a 450 mW integral Sterling CLOSED-CYCLE cooler assembly (shown in Fig. 8) and installed into an Amber RADIANCE 1 ™ camera-body, to demonstrate a hand-held 1.WIR camera (shown in Fig. 9). The camera is equipped with a 32-bit floating-point digital signal processor combined with multi-tasking software, providing the speed and power to execute complex image-processing and analysis functions inside the camera body itself. The other element of the camera is a 100 mm focal length germanium lens, with a 5.5 degree field of view, It is designed to be transparent in the 8-12 pm wavelength range, to be compatible with the QWIP's 8.5 µm

operation. The digital acquisition resolution of the camera is 12-bits. Its nominal power consumption is less than 50 Watts.

The measured mean NEΔT of the QWIP camera is 40 mK (the higher NEΔT is due to the lens assembly cutting the light transmission by 35%) at an operating temperature of T = 70 K and bias V_B = -1.5 V, for a 300 K background. The peak quantum efficiency of the FPA is 3%, corresponding to an average of 3 passes of IR radiation through the photosensitive multi-quantum well region. The low quantum efficiency can be partly attributed to the fact that the substrate reflects 30% of the light striking it; and the fact that the array has a 65% fill factor, i.e., the detectors cover only 65% of the array surface, with the remaining 35% being the dead space between detectors. The uncorrected photocurrent non-uniformity (which includes a 1 % non-uniformity of the ROC and a 1 .4% non-uniformity due to the cold-stop in front of the FPA not yielding the same field of View to all the pixels) of the 65,536 pixels of the 256x256 FPA is about 6.8% (= signm/mean). The non-uniformity after two-point (17° and 27° Celsius) correction improves to an impressive 0.05%. As mentioned earlier, this high yield is due to the excellent GaAs growth uniformity and the mature GaAs processing technology.

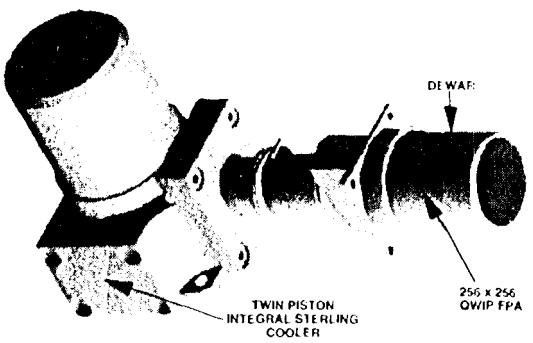

Fig. 8 Picture of the QWIP camera's sensor engine, which combines advanced 256x256 QWIP FPA and twin piston integral Sterling cooler. This cooler is capable of providing cooling capacities exceeding 450 mW at 70 K in a standard room temperature environment of 23°C.

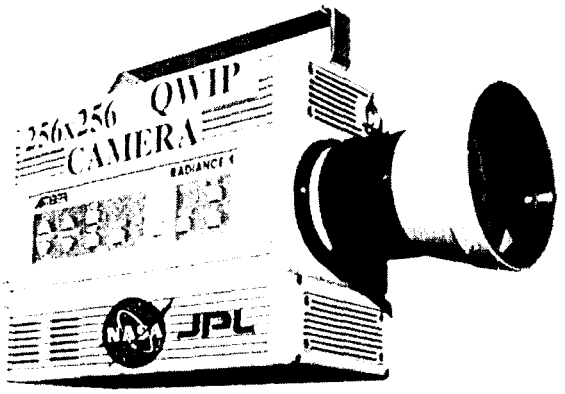

Fig. 9 Picture of the first 256x256 hand-held long wavelength QWIP camera (QWIP RADIANCE).

Video images were taken at a frame rate of 60 Hz at temperatures as high as T = 70 K, using a ROC capacitor having a charge capacity of 9x10~ electrons (the maximum number of photoelectrons and dark electrons that can be counted in the time taken to read each detector pixel). Figure 10 (a) shows one frame of a video image taken with a 9 μm cutoff 256x2,56 QWIP camera. The two tiny dark squares on the glasses are reflections of the cold FPA of the came.ra, i.e., the QWIP FPA is imaging itself in the infrared mirror that each frame of the man's glasses constitutes! Figure 1 O(b) shows an absorption image of acetone fames (acetone has a strong IR absorption at 8.8 μm) taken with the same camera. These images demonstrate the high sensitivity of the 256x256 QWIP staring array camera.

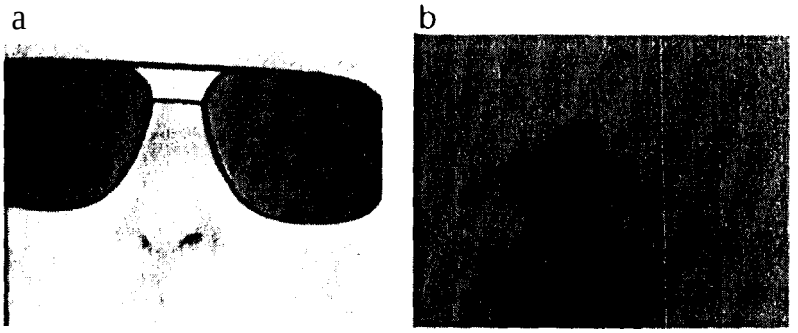

Fig. 10. Schematic diagram of the conduction band in a bound-to-continuum QWIP in an externally applied electric field. Absorption of IR photons can photoexcite electrons from the ground state Of the quantum well info the continuum, causing a photocurrent. Three dark current mechanisms are also shown: ground state tunneling (1); thermally assisted tunneling (2); and thermionic emission (.?).

SUMMARY

Exceptionally rapid progress has been made in the development of long wavelength QWIPs, since they were first experimentally demonstrated several years ago. It is now possible for QWIPs to achieve excellent performance (e.g., detectivities as high as $D^* \sim 1x10^{11}$ cm√Hz/W at 70 K for a 9 μm QWIP) and be fabricated into large inexpensive low-noise imaging arrays. A 70 K operating temperature can be easily achieved by single-stage Stirling cycle coolers, which allows us to demonstrate the first hand-held 2.56x256 FPA LWIR camera based on QWIPs. Weighing about ten pounds, the QWIP RADIANCE 1 camera is entirely self-con(aincd, with no extra boxes for control, cooling, or image processing. Its sharp, inexpensive, large, uniform, infrared cyc (which can be tailored to scc a particular 1 R wavelength) makes the QWI f' hand-held camera the best and the most cost-effective new tool for imaging and spectroscopy in the interesting 8-14 pm wavelength range..

ACKNOWLEDGMENTS

The research described in this paper was performed by the Center for Space Microelectronics Technology, Jet Propulsion 1 aboratory, California Institute of Technology, and was jointly sponsored by the BMDO/IS&T Office, and the NASA Office of Space Access and Technology.

REFERENCES

[1] M. '1'. Chahine, "Sensor requirements for Earth and Planetary Observat ions, " Proceedings *of Innovative Long Wavelength Infrared Detector Workshop,* Pasadena, California, pp. 3-31, April 24-26, 1990.

[2] D. Duston, "BMDO's IS&T faces new hi-tech priorities," *BMD Monitor, pp. 180-183,* May 19, 1995.

[3] C. G. Bethea, B. F. Levine, M. 'I'. Asom, R. E. Leibenguth, J. W. Stayt, K. G. Glogovsky, R. A. Morgan, J. D. Blackwell, and W. J. Parrish, "I .ong Wavelength Infrared 128 x 128 AlxGa1 - xAs/GaAs Quantum Well Infrared Camera and imaging System, " *IEEE Trans. Electron. Devices*, vol. 40, pp. 1957-1963, 1993.

[4] 1.. J. Kozlowski, G. M. Williams, G. J. Sullivan, C. W. Farley, R. J. Andersson, J. Chen, D. '1'. Cheung, w. E. Tennant, and R. E. DeWames, "1 .WIR 128x 128 GaAs/AlGaAs Multiple Quantum Well Hybrid Focal Plane Array," *11<1<1<7 rans. Electron. Devices*, vol. Ire-38, pp. 1124-1130, *1991.*

[5] W. A. Beck, T. S. Faska, J. W. Little, J. Albritton, and M. Sensiper, *Proceedings of the Second international Symposium on* 2-20 *µm Wavelength Infrared Detectors and* A *rrays: Physics and Applications*, October 10-12, 1994, Miami Beach, Florida.

[6] B. F. Levine, C. G. Bethea, G. Hasnain, V. O. Shen, E. Pelve, R. R. Abbott, and S, J. Hsieh, "1 ligh sensitivity low dark current10 pm GaAs quantum we.]] infrared photodetectors," *Appl. Phys. Lett.*, vol. S6, pp. 851-853, 1990.

[7] S. D. Gunapala and K. M. S. V. Bandara, Physics of Thin Films, Academic Press, 21, 113 (1 995), *and references therein.*

[8] Sarath Gunapala, Gabby Sarusi, Jin Park, "1 'rue-] .on I in, and Barry Levine, "Infrared Detectors Reach Ncw Lengths," *Physics World*, pp. 35-40, December, 1994.

[9] S. D. Gunapala, J. S. Park, G. Sarusi, "1'. L. Lin, J. K. Liu, P. D. Maker, R. E. Muller, C. A. Shott, '1'. Hoelter, and B. F. Levine " 128 x 128 GaAs/$Al_xGa_{1-x}As$ Quantum Well Infrared Photodetector Focal Plane Array for Imaging at 15 µm," submitted to *IEEE Electron De vice Letters.*

[10] W. A. Beck, "Photoconductive gain and generation-recombination noise in multiple-quantum-well infrared detectors," *Appl. Phys. Lett.*, vo]. 63, pp. 3589-3591, 1993.

[11] G. Sarusi, B. F. Levine, S. J. Pearton, K. M. S. V. Bandara, and R. E. Leibenguth, "Improved performance of quantum well infrared photodetectors using random scattering optical coup ling," *Appl. Phys. Lett., VOI. 64, pp. 960-962, 1994.*